Model for Estimating Radiated Emissions From a Printed Circuit Board With Attached Cables Due to Voltage-Driven Sources

Hwan-Woo Shim and Todd H. Hubing, *Senior Member, IEEE*

***Abstract*—Common-mode currents induced on cables attached to printed circuit boards (PCBs) can be a significant source of unintentional radiated emissions. This paper develops a model for estimating the amount of common-mode cable current that can be induced by the signal voltage on microstrip trace structures or heatsinks on a PCB. The model employs static electric field solvers or closed-form expressions to estimate the effective self-capacitances of the board, trace, and/or heatsink. These capacitances are then used to determine the amplitude of an equivalent common-mode voltage source that drives the attached cables. The model shows that these *voltage-driven* common-mode cable currents are relatively independent of the cable parameters and the trace or heatsink location when the PCB is small relative to the cable length and to a wavelength.**

***Index Terms*—Absolute capacitance, current-driven radiation, radiated emissions, radiation by attached cables, voltage-driven radiation, wire antenna.**

I. Introduction

COMMON-MODE currents induced on cables attached to printed circuit boards (PCBs) are a well-known source of unintentional radiated emissions [1]–[5]. The mechanisms by which intentional signals induce common-mode currents on attached cables can generally be divided into two categories: *current-driven* (coupled from the signal's magnetic field) and *voltage-driven* (electric field coupled) [6]. Examples of these coupling mechanisms are illustrated in Fig. 1.

In Fig. 1(a), the current-driven mechanism is associated with the magnetic fields that wrap around the finite width of the signal return plane. The effective voltage drop across the plane induces common-mode currents on the cables. The induced common-mode current is directly proportional to the signal current. If there are two cables connected to opposite sides of the board, they are driven like a dipole antenna. The current-driven mechanism has been observed to be a dominant source of radiated emissions and has been studied by many researchers [2], [3], [6]–[10]. Several researchers have proposed methods to calculate the effective inductance of the return plane for the purpose of calculating the induced common-mode currents [7]–[10]. Experimental studies have shown that the current-driven model in Fig. 1(a) provides reasonable estimates of the induced common-mode currents and radiated fields [11], [12].

Manuscript received August 20, 2004; revised August 22, 2005.

H.-W. Shim is with the Mobile Communication Division, Samsung Electronics Company, Gumi-city Gyeong-buk, Korea 730-350.

T. H. Hubing is with the Department of Electrical Engineering, University of Missouri–Rolla, Rolla, MO 65409 USA (e-mail: hubing@umr.edu).

Digital Object Identifier 10.1109/TEMC.2005.859060

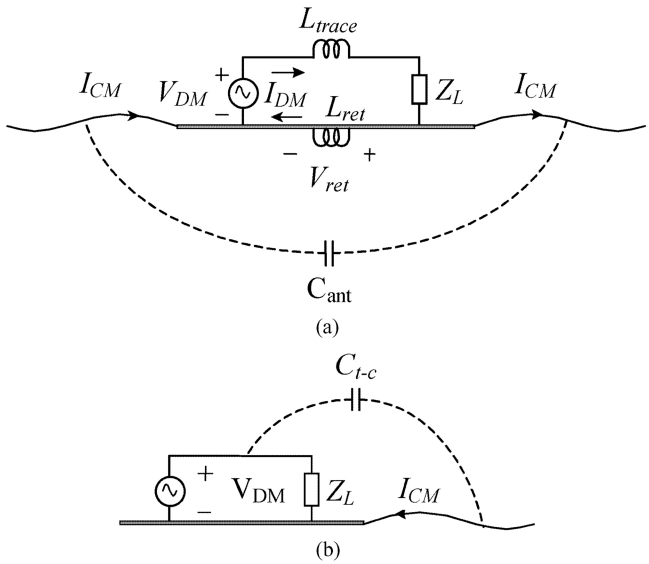

Fig. 1. Basic coupling mechanisms for inducing common-mode current on attached cables: (a) current-driven and (b) voltage-driven.

The electric fields that couple directly to attached cables, as illustrated in Fig. 1(b), can also induce common-mode currents. This source mechanism is referred to as voltage driven because the magnitude of the common-mode current is proportional to the signal voltage. Although current-driven sources typically drive objects referenced to the same "ground" against each other, voltage-driven sources typically drive objects referenced to "ground" against other objects whose potentials are related to the signal voltage. At a minimum, the object typically being driven consists of the signal trace itself. If the signal trace capacitively couples to another larger object (e.g., a heatsink), the voltage-driven emissions can be significantly enhanced. Assuming voltage-driven radiation is apparent only when there is at least one large ungrounded metallic structure on the board, the voltage-driven mechanism has received relatively little attention in the literature. In this paper, it is shown that this voltage-driven mechanism can be a significant source of radiated emissions, and a model for estimating voltage-driven common-mode currents is developed. The goal of this work was to develop a model that could be used by electromagnetic compatibility expert systems [23], [24] to anticipate and quantify possible radiated emissions problems due to voltage-driven, common-mode currents on cables. The model was required

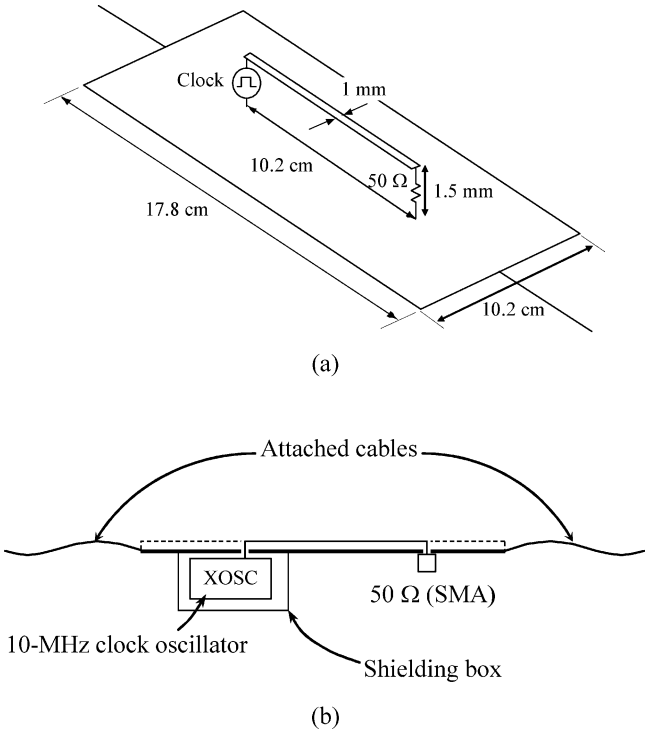

Fig. 2. Test board configuration: (a) perspective view and (b) side view.

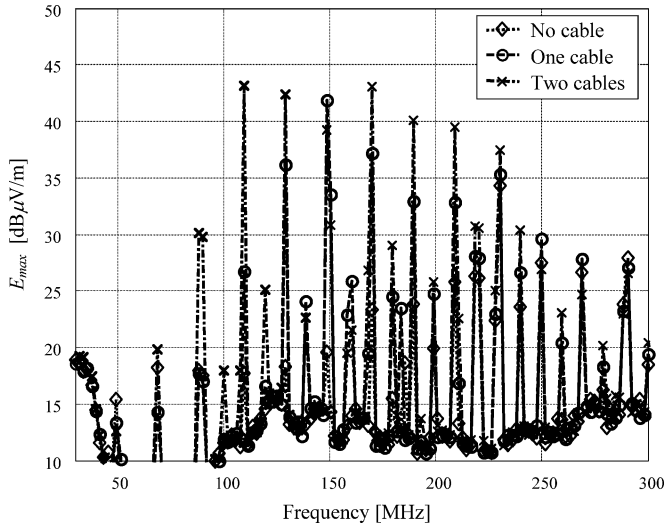

Fig. 3. Measured radiated emissions from test board.

to employ a closed-form expression to estimate the maximum likely emissions from typical PCB structures.

This paper is organized as follows. Section II demonstrates the importance of voltage-driven radiation both experimentally and numerically. A wire antenna model for voltage-driven radiation is introduced in Section III. In Section IV, the model is applied to two different geometries; a voltage on a signal trace and a heatsink driven against a signal return plane. The radiated emissions from simplified antenna models are compared with the emissions from the full configurations.

II. Importance of Voltage-Driven Radiation

A. Experimental Comparison of Radiated Fields

To compare the intensity of the radiated fields generated by current- and voltage-driven sources, a simple test board was built, and the radiated emissions were measured in a semianechoic chamber. The test board configuration is illustrated in Fig. 2. The 10.2×17.8 cm PCB had a 1-mm-wide 10.2-cm-long trace at the center of the board. The board had one trace and one solid return plane separated by 1.5 mm of dielectric material that had a relative permittivity of approximately 4.3. The trace was driven by a 10-MHz clock oscillator that was located on the bottom side of the solid plane and powered by batteries. Both the clock oscillator and the batteries were covered with a shielding box to prevent direct radiation.

The attached cables were 50 cm long and connected to each side of the board as shown in Fig. 2. The output pin of the oscillator was connected to one end of the trace, and the other end of the trace was terminated with a 50-Ω resistor using an SMA connector. Due to the trace inductance, which was about 43 nH [13], the differential-mode current $I_{\rm DM}$ was not in phase with the voltage $V_{\rm DM}$ at high frequencies. However, the current distribution along the trace was nearly uniform up to 300 MHz, where the trace was electrically short. The board was placed on a 0.8-m tall wooden table that was rotated to detect the maximum emissions. The receiving antenna was horizontally polarized (i.e., in the plane of the board). The measured radiated field at a distance of 3 m is shown in Fig. 3.

As expected at harmonic frequencies below 250 MHz, where the board length is much shorter than the wavelength, the measured fields without attached cables are much weaker than those with attached cables. When two cables are connected, the current-driven mechanism drives the two cables against each other and is the dominant source of radiated emissions. The measurement shows that the radiated fields with two attached cables are highest over most of the frequency range up to 250 MHz, except for the peak at 150 MHz. With one cable attached, removing the 50-Ω load from the circuit causes most of the emission peaks (including the peak at 150 MHz) to increase by several decibels, indicating that a voltage-driven mechanism is responsible for this radiation. This result experimentally demonstrates that emissions due to voltage-driven, common-mode currents can be just as important as emissions due to current-driven, common-mode currents, even when the only structure being driven at the signal voltage is a microstrip trace.

B. Numerical Comparison of Radiated Fields

To further investigate the role of the two source mechanisms, a numerical simulation was performed. The configuration modeled was similar to that of the experimental test board and is illustrated in Fig. 4. This board is 10×4 cm and has a 5-cm-long trace at the center. The height and the width of the trace are both 1 mm. An ideal 1-V source is connected to one end of the trace. The other end is terminated with a 50-Ω resistor. 50-cm cables were connected to each end of the board. The maximum

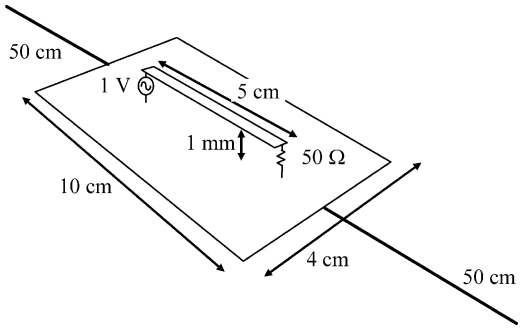

Fig. 4. Field solver test board configuration

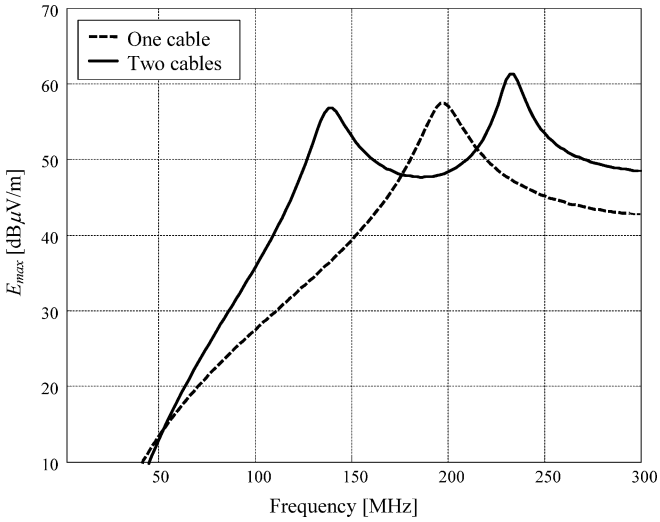

Fig. 5. Calculated intensity of radiation from test board.

radiated field was calculated at a distance of 3 m from the center of the board. The board was located in free space without a conducting floor. The horizontal electric field was calculated 0–3 m above the plane in 20-cm increments and around the board in increments of 5 degrees. All full-wave simulations in this article were performed using a moment-method field solver called COMORAN [15].

The calculated maximum electric field strength is shown in Fig. 5. The board with two attached cables exhibits resonances at 139 and 233 MHz, indicating that one cable is being driven relative to the other. This suggests that the current-driven source mechanism is dominant. When only one cable is connected to the board, there is a peak at 197 MHz. The magnitude of this peak is comparable to those due to the current-driven mechanism, but calculations based on a current-driven model do not predict a peak this strong [24].

C. Identifying the Radiation Sources

The boards that were measured had a shielding box covering the clock oscillator and batteries. There was no other metallic structure against which the potential drop on the reference plane could drive the cable. To verify that the radiation peak with one cable is proportional to the signal voltage V_{DM}, three configurations of the simulation test board are modeled as shown in Fig. 6. By modifying the source and load resistances, the trace voltage and current can be varied independently. The geometry of the board is the same as that shown in Fig. 4.

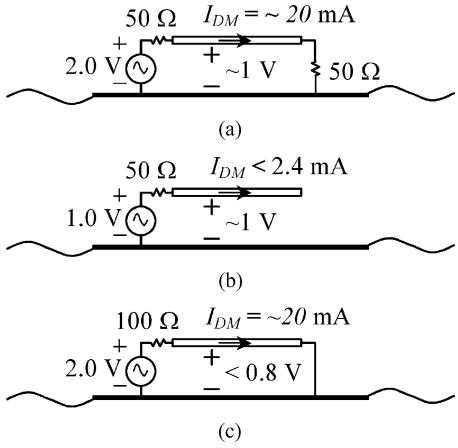

Fig. 6. Three different configurations to identify cable coupling mechanisms: (a) loaded microstrip trace, (b) voltage-driven source, and (c) current-driven source.

The inductance of the trace is about 21 nH [25], and the corresponding reactance at 300 MHz is about 40 Ω. For the original configuration shown in Fig. 6(a), the trace current ranges between 19 and 20 mA, and the trace voltage is about 1 V over the frequency range of interest. Because the trace is electrically short, the current and voltage distributions along the trace are relatively uniform. The configuration shown in Fig. 6(b) is open at the load end. The trace capacitance is about 1.3 pF. Because the reactance associated with the trace capacitance is much greater than the 50-Ω source resistance, the trace voltage is about 1 V. The current on the trace is about 2.4 mA at 300 MHz, which is much smaller than that of the original configuration. The radiation due to the voltage-driven mechanism, therefore, should be similar to that of the original configuration with far less current-driven radiation. The current-driven configuration shown in Fig. 6(c) has a similar amount of current on the trace as the original configuration. However, the trace voltage ranges between 0 and 0.8 V, depending on the frequency due to the trace inductance, which is less than the original configuration. Thus, the radiation due to the current-driven mechanism should be similar to that of the original configuration, whereas the voltage-driven radiation should be lower. The maximum radiated fields at a distance of 3.0 m from the board were calculated from 30 to 300 MHz.

The results plotted in Fig. 7 indicate that the emissions from the original 50-Ω configuration can be divided into two components: a voltage-driven component and a current-driven component. The current-driven radiation peaks at 139 MHz (the half-wave resonance of the board driving one cable relative to another). The voltage-driven radiation peaks at 233 MHz (the half-wave resonance of the board being driven relative to the cables). The radiation from the original configuration exhibits both resonances. There is a small peak at 139 MHz for the voltage-driven configuration due to the small amount of current flowing through the trace. Because the trace capacitance is about 1.3 pF [25], the differential-mode

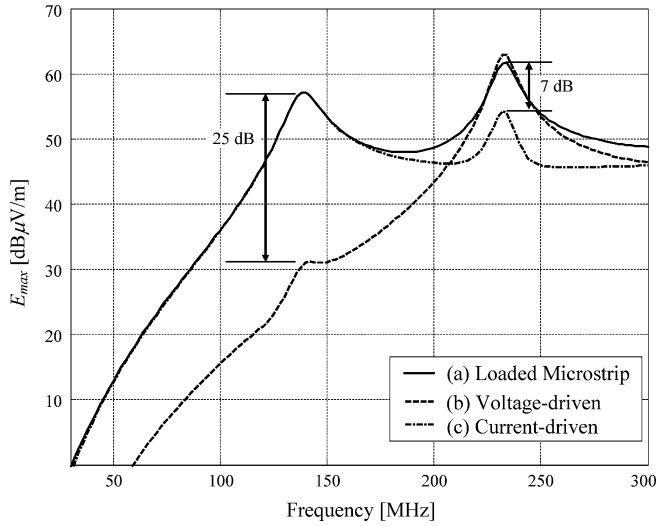

Fig. 7. Simulated emissions from test board with different configurations.

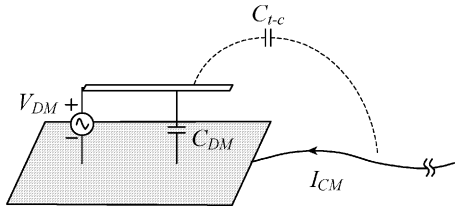

Fig. 8. Voltage-driven coupling to attached cable.

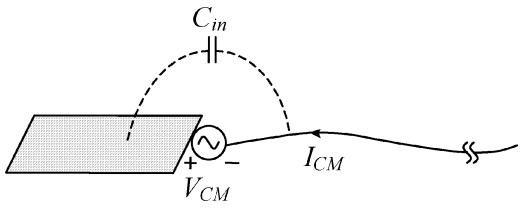

Fig. 9. Equivalent wire antenna model for voltage-driven coupling.

current is about 1.1 mA at that frequency. This is about 25 dB $[\approx 20\log(20/1.1)]$ less than the current in the original configuration. Similarly, the current-driven configuration has a small peak at 233 MHz, where voltage-driven peaks are dominant. This is caused by the trace inductance, which creates a voltage on the trace of about 0.59 V at 233 MHz. Note that the potential distribution on the trace is not uniform in the current-driven configuration. The trace potential at the source end is 0.59 V and nearly 0 V at the load end. Thus, the average trace voltage is less than 0.59 V, creating a more than 4.6 dB $[\approx 20\log(1.0/0.59)]$ difference at 233 MHz.

Note that the radiation peaks due to both mechanisms are comparable, even though there are no large metallic structures on the board for the voltage-driven source mechanism to drive. These results suggest that the radiation from voltage-driven sources should not be neglected when estimating the radiated emissions from PCBs with attached cables.

III. Voltage-Driven Source Model

A. Simplified Antenna Model

The common-mode current on cables driven by a voltage-driven source is induced by the electric fields that couple to cables from traces or other structures. Fig. 8 illustrates the voltage-driven mechanism in its simplest form. Assuming the board is electrically small, the electric fields coupled to the attached cable can be represented by an effective mutual capacitance between the trace and the cable C_{t-c}.

The signal voltage source $V_{\rm DM}$ drives a differential-mode current that flows out on the trace and back on the plane. However, the common-mode current flowing on the cable is primarily responsible for the radiated emissions. The conversion from differential- to common-mode can be modeled by placing equivalent common-mode voltage sources at locations where there is a change in the "balance" of the structure [21] and [22]. In this case, the dominant effective common-mode source occurs at the junction between the cable and the plane as illustrated in Fig. 9.

In general, the input impedance of a wire antenna heavily depends on its location along the wire. The current distribution, however, is approximately the same for any source position electrically close to one end of the wire. This means that the radiation from a wire antenna is independent of the source location if we adjust the magnitude of the source to keep the magnitude of the induced common-mode current the same. If the length of the attached cable in Fig. 8 is much longer than the board, the radiated emissions are dominated by the common-mode current on the cable and the effect of the common-mode current on the other parts of the antenna is negligible. Thus, the radiation from the board can be calculated by modeling the system as a wire antenna with an equivalent common-mode voltage source. The magnitude of the source must be adjusted so the induced common-mode current is the same as that in the original configuration.

For the original configuration in Fig. 8, the induced charge on the cable is given by $C_{t-c}V_{\rm DM}$, whereas that of the equivalent wire antenna model in Fig. 9 is $C_{\rm in}V_{\rm DM}$. Therefore, the magnitude of the common-mode voltage source can be expressed as

$$V_{\rm CM} = \frac{C_{t-c}}{C_{\rm in}} V_{\rm DM} \tag{1}$$

where C_{t-c} is the effective mutual capacitance between the trace and the attached cable, and $C_{\rm in}$ is the input capacitance of the wire antenna model.

B. Input Capacitance of the Wire Antenna Model

Assuming the board is electrically small, the equivalent circuit model shown in Fig. 10 can be used to derive the input capacitance of the antenna model. The input capacitance is the parallel connection of the mutual capacitance between the board and cable C_M and the two self-capacitances of the cable and board in series. Because the cable is much longer than the board, the series connection of two self-capacitances is approximately

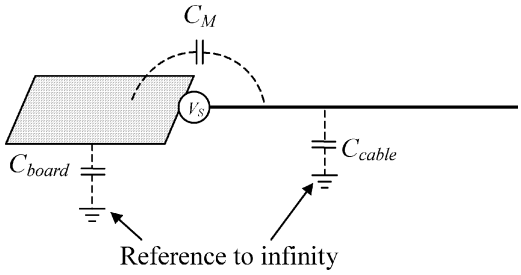

Fig. 10. Equivalent circuit for wire antenna model.

equal to the board's self-capacitance C_{board}

$$C_{\text{in}} = C_M + \frac{C_{\text{board}} \cdot C_{\text{cable}}}{C_{\text{board}} + C_{\text{cable}}} \approx C_M + C_{\text{board}}. \quad (2)$$

The mutual capacitance C_M is associated with the electric fields that originate from the board and directly couple to the cable. The length and thickness of the cable determine the mutual capacitance and affect the magnitude of induced current near the source. The directly coupled electric fields are concentrated near the edge of the board, and the geometry of the cable has a strong impact on the capacitance for a short cable. For a long cable, however, the total amount of induced charge on the cable weakly depends on the mutual capacitance. If the cable is thin and much longer than the board dimensions, the mutual capacitance is much smaller than the board capacitance C_{board}. Thus, for typical board-cable geometries, the magnitude of the induced current is limited by the board capacitance C_{board}, not by the mutual capacitance C_M. This implies that the mutual capacitance can be neglected for a long attached cable, and the input capacitance of the antenna model can be approximated by the self-capacitance of the board. The self-capacitance of a rectangular plane is similar to that of a circular disc of the same area, which is approximately $8\varepsilon_o r$, where r is the radius of the disc [14]. Therefore, the input capacitance of the wire antenna model can be approximated as

$$C_{\text{in}} \approx C_{\text{board}} \approx 8\varepsilon_o \sqrt{\frac{\text{Board Area}}{\pi}}. \quad (3)$$

Full-wave simulations were used to check the accuracy of (3). Assuming the dimensions of the system are electrically small, the current induced on the attached cable at the source position is determined by the input capacitance as $I_{\text{cable}} \approx 2\pi f C_{\text{in}} V_{\text{CM}}$. Therefore, the capacitance is given by

$$C_{\text{in}} \approx \frac{1}{2\pi f} \left| \frac{I_{\text{cable}}}{V_{\text{CM}}} \right| \quad (4)$$

where I_{cable} is the magnitude of the induced current on the cable at the source position, and V_{CM} is the magnitude of the voltage source that drives the system. A configuration similar to the one in Fig. 9 was simulated. The board was 4 cm wide and 10 cm long. The source amplitude was 1 V at 1 MHz. The wavelength at 1 MHz is about 300 m, which is much greater than the cable length and the dimensions of the board. The effects of length and thickness of the cable were investigated. Fig. 11(a) shows the currents induced on the cable when the length of the

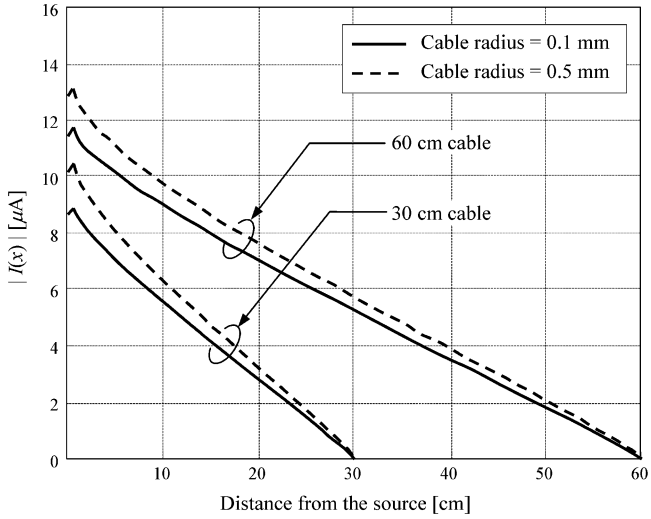

(a)

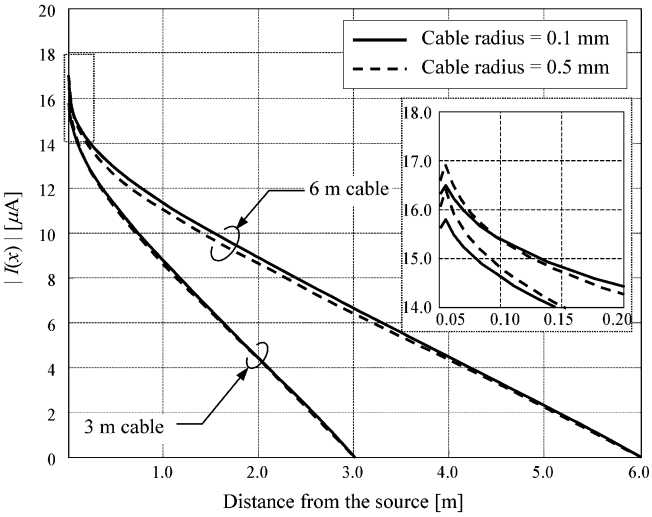

(b)

Fig. 11. Distribution of current along cable at 1 MHz, where length of cable is: (a) comparable to and (b) much longer than board dimensions.

cable is comparable to the board dimensions. In this case, the magnitude of the current at the source position depends on both the length and the thickness of the cable, which implies that a significant portion of the current is determined by the mutual capacitance between the cable and the board. However, the results for longer cables shown in Fig. 11(b) shows that the magnitude remains almost the same regardless of the cable length and thickness, indicating that the effect of the mutual capacitance is negligible.

If the cable is long enough, the current is limited by the board capacitance because the cable capacitance is much greater. Table I compares the effective self-capacitance of the board estimated using the simple closed-form expression (3) to the antenna input capacitance derived from numerical simulations. The results show that the antenna input capacitance is within 1.5 dB of the board self-capacitance estimate for all configurations evaluated. These simulations verify that the magnitude of the induced current on the

TABLE I
COMPARISON OF BOARD SELF-CAPACITANCE C_{BOARD} (3) AND INPUT CAPACITANCE C_{IN} BETWEEN BOARD AND 10-m-LONG CABLE (FROM SIMULATION)

Board area [cm^2]	40			60		
C_{board} [pF]	2.53			3.10		
L [cm]×W [cm]	10 × 4	8 × 5	6.7 × 6	12 × 5	10 × 6	8 × 7.5
C_{in} [pF]	2.64	2.61	2.59	3.66	3.17	3.14

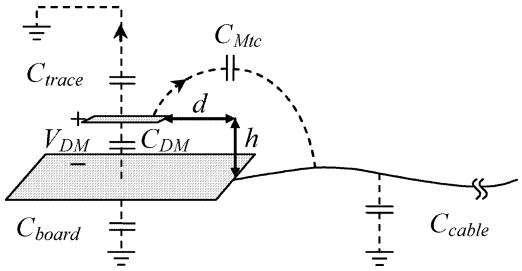

Fig. 12. Effective capacitances of PCB with attached cable.

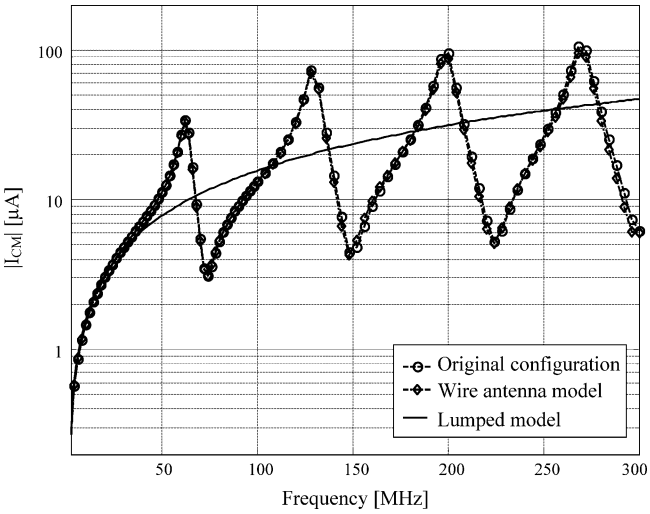

Fig. 13. Comparison of induced common-mode currents on attached cable.

attached cable was determined primarily by the board capacitance for the configurations evaluated. If the cable is thin and much longer than the board dimensions, the input capacitance of the antenna model is approximately equal to the board capacitance.

C. Effective Mutual Capacitance Between the Trace and Attached Cable

Because the amount of the common-mode current on an attached cable driven by the trace voltage V_{DM} is directly proportional to the effective mutual capacitance between the trace and the cable, this capacitance is a critical parameter for the voltage-driven mechanism. To better understand this capacitance, it is helpful to refer to the model shown in Fig. 12. C_{DM} is the mutual capacitance between the trace and the signal return plane. This contributes to the differential-mode current that returns to the source through the plane. The self-capacitances of each conductor representing the stray electric field lines that terminate at infinity are also shown in the circuit. C_{Mtc} is the mutual capacitance representing electric field lines that directly link the trace and cable.

As indicated in Fig. 1(b), the amount of common-mode current on the cable is determined by the effective mutual capacitance C_{t-c} between the trace and the attached cable. Fig. 12 illustrates that this effective mutual capacitance is the parallel combination of the mutual capacitance C_{Mtc} and the series combination of the self-capacitances C_{trace} and C_{cable}.

C_{Mtc} can be viewed as representing the lines of electric flux that originate on the trace and terminate on the cable. C_{trace} and C_{cable} represent lines of electric flux that originate on the trace or cable, respectively, and terminate at infinity. If the attached cable is thin and the trace is located away from the edge, the mutual capacitance C_{Mtc} is much smaller than the series combination of C_{trace} and C_{cable}. This is the case for most typical configurations, and the amount of common-mode current is determined by the equivalent capacitance of the current path through C_{trace} and C_{cable}. Because the length of the cable is much greater than the length of the trace in general, $C_{\mathrm{trace}} << C_{\mathrm{cable}}$. Thus, the common-mode current on the cable is limited primarily by the trace capacitance and the effective mutual capacitance associated with the common-mode current path can be approximated as

$$C_{t-c} \approx C_{\mathrm{trace}}. \tag{5}$$

Using this approximation, the expressions for the amplitude of the equivalent common-mode voltage source in (1) can be rewritten as

$$V_{\mathrm{CM}} \approx \frac{C_{\mathrm{trace}}}{C_{\mathrm{board}}} V_{\mathrm{DM}}. \tag{6}$$

C_{trace} can be determined using a static field solver or a closed-form approximation, whereas C_{board} is the board capacitance provided in (3).

This equation and the simple model in Fig. 9 provide an efficient way to estimate the radiation from the board. A three-dimensional (3-D) full-wave simulation of a PCB usually requires a large amount of computational resources. However, the model shown in Fig. 9 is relatively simple, taking far less time and resources to simulate.

IV. VALIDATION OF THE ANTENNA MODEL

A. Comparison of Common-Mode Current

To validate the equivalent model described in the previous section, the common-mode currents induced on cables attached to a board were calculated using a full-wave simulator and compared with wire antenna model estimates. The capacitances for the wire antenna model were calculated using *FastCap*, a 3-D capacitance extraction program developed by the Research Laboratory of Electronics at the Massachusetts Institute of Technology and based on an accelerated boundary element technique [16].

The test geometry was similar to one in Fig. 4, except that the load end was open to minimize the current on the trace. The

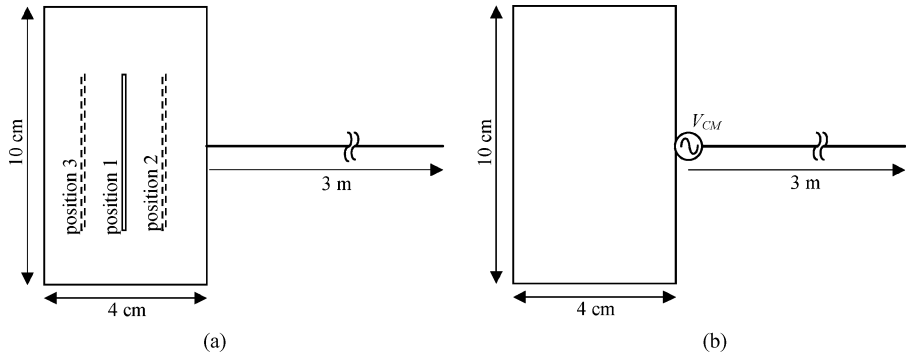

Fig. 14. Test board configurations: (a) original board and (b) corresponding antenna model for voltage-driven mechanism.

board was 10×4 cm and had one 5-cm-long trace, which was 1 mm wide and positioned 1 mm above the center of the plane. A 1-m-long cable was attached to the board, and the radius of the cable was 0.5 mm. To calculate the radiated emissions from the original configuration, a 1-V voltage source was connected between the trace and the return plane. There was no dielectric material between the trace and the return plane. The dielectric has little effect on the value of $C_{\rm trace}$ for typical PCB configurations [26].

The self-capacitance of the trace and the board were calculated using *FastCap*. They were 0.025 and 2.57 pF, respectively. Applying these capacitance values to (6) suggests that a 1-V signal amplitude generates a 9.7-mV common-mode voltage. A full-wave solver was used to simulate the original configuration, including the board, cable, and trace. The same solver was then used to simulate the wire antenna model in Fig. 9 with a 9.7-mV source. The calculated currents induced on the cable near the board are shown in Fig. 13. The calculated common-mode current based on a simple lumped model

$$|I_{\rm CM}| \approx 2\pi f C_{\rm trace} |V_{\rm DM}| \tag{7}$$

is also shown. The results agree well with each other at low frequencies, where the dimensions of the board and the cable are electrically small. The lumped element model starts to deviate due to the cable resonance at about 40 MHz. However, the wire antenna model results agree well with the original configuration results over the entire frequency range.

B. Radiation Due to a Trace Voltage

According to the wire antenna model presented in the previous sections, the currents induced on the attached cable depend on the trace capacitance, but not on the trace position. To verify this, boards were evaluated with different trace positions. Fig. 14(a) shows a 4×10 cm test board with a 3-m-long cable attached to the end. The 1-mm-wide trace is 5 cm long, which is electrically short over the frequency range of the interest, and is 1 mm above the plane. A 1-V source is connected to the center of the trace, and no loads are connected to the trace. Because there was only one attached cable and it was perpendicular to the trace, any differential-mode current (which should be small because the end of the trace was open) creates a potential drop along the longitudinal direction of the board and does not induce a significant amount of common-mode current on the attached cable. As shown in Fig. 14(a), three different positions of the trace were considered for the simulations. The corresponding wire antenna model is illustrated in Fig. 14(b). In the antenna model, the source is replaced by a common-mode voltage source $V_{\rm CM}$, whose amplitude is given by (6). Using *FastCap*, the board capacitance was found to be 2.67 pF for position 1 and 2.66 pF for positions 2 and 3. The self-capacitance of the trace was 0.026 pF for position 1 and 0.03 pF for positions 2 and 3. Based on these values, the equivalent wire antenna model should employ a common-mode voltage source of 9.7 mV for position 1 and 11.3 mV for positions 2 and 3. For convenience, the magnitude of the common-mode voltage source of the wire antenna model was set to 10 mV for all positions. The radiated field intensities at a distance of 10 m were calculated using a full-wave solver and are shown in Fig. 15. The results show that the radiated field strengths agree well at frequencies up to 300 MHz, indicating that the position of the trace was not a significant factor.

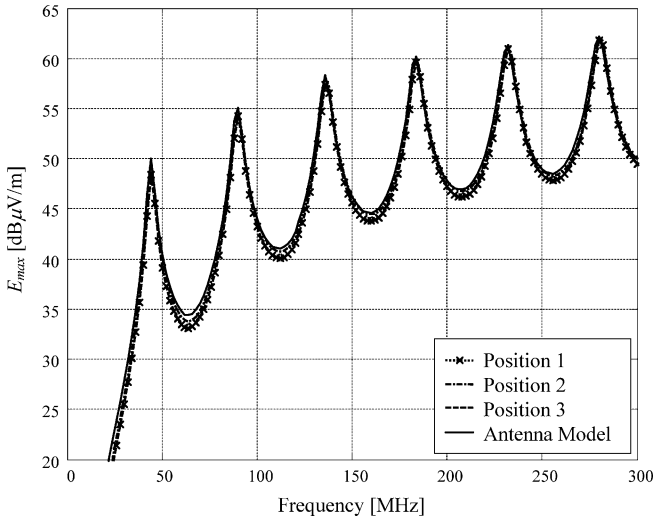

Fig. 15. Comparison of radiated field intensity from full configuration and corresponding antenna model.

C. Radiation Due to a Heatsink

Relatively small heatsinks, such as microchip heatsinks, have resonant frequencies well above 1 GHz [17]–[20]. Thus, the

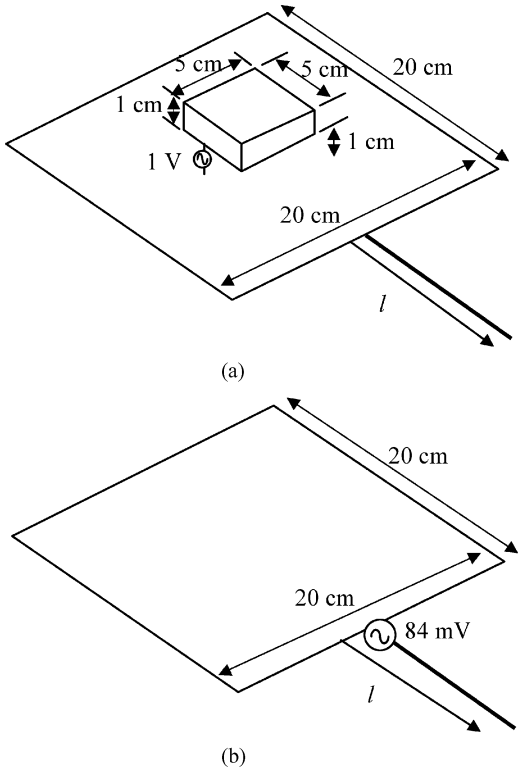

Fig. 16. Illustration of test board: (a) original configuration and (b) corresponding antenna model.

radiation below 1 GHz is more likely to be dominated by the resonances of the attached cables rather than the heatsinks. However, heatsinks can play a significant role in voltage-driven cable radiation. If a board is electrically small and the self-capacitance of the heatsink is smaller than that of the board, the previous simplified model can be used to estimate the radiated emissions. The self-capacitance of the heatsink can be calculated using 3-D static field solvers or estimated using closed-form expressions.

A simple board was designed to validate the wire antenna model for a PCB with a heatsink. The board configuration is shown in Fig. 16. A $5 \times 5 \times 1$ cm heatsink is located 1 cm above the plane at the center of the board. A 1-V voltage source drives the heatsink against the plane. A 1-m-long cable is attached to the plane. The self-capacitance of the heatsink above the plane without the attached cable was calculated using *FastCap* and found to be 0.43 pF. The self-capacitance of the plane was 5.14 pF. Applying these values to (6), the equivalent common-mode source voltage was found to be 84 mV. The corresponding simplified antenna model is shown in Fig. 16(b).

The maximum radiated fields from both the original configuration and the simplified model were calculated using a full-wave simulation at frequencies up to 300 MHz. The results are shown in Fig. 17. The maximum electric field strength was calculated at a distance $r = 3$ m from the board with a 1-m attached cable and 10 m from the board with a 3-m attached cable. In both cases, the radiated field from the original configuration and the wire antenna model agree well at frequencies up to 180 MHz. The results start to deviate above 200 MHz as the length of the board becomes comparable to the wavelength, but are within a few decibels up to 300 MHz.

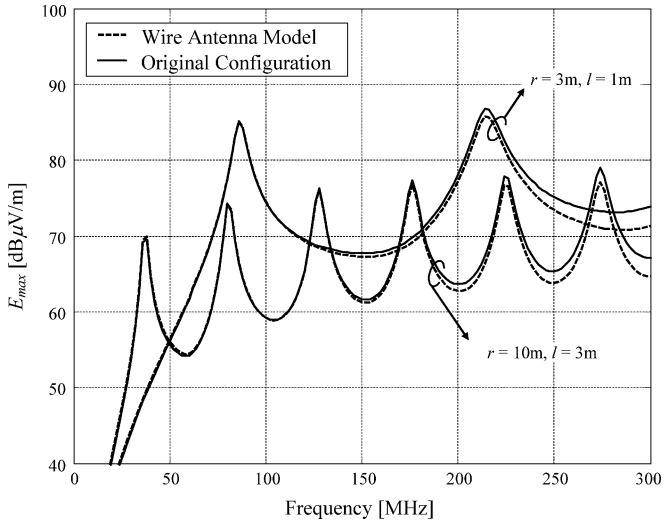

Fig. 17. Comparison of simulated emissions from original configuration and wire antenna model of heatsink on PCB.

V. Conclusion

In this paper, an equivalent wire antenna model has been developed to estimate the radiated emissions from PCBs with attached cables when common-mode currents are induced on the cables via a voltage-driven radiation mechanism. The magnitude of the equivalent common-mode voltage source that drives the antenna is expressed in terms of the ratio of the self-capacitances of metallic structures on the board. These capacitances can be calculated using a static field solver or approximated using closed-form expressions. It was shown that this technique can be used to estimate radiated fields well beyond the first resonant frequencies of the attached cables as long as the board dimensions are electrically small.

References

[1] C. R. Paul, "A comparison of the contribution of common-mode and differential-mode currents in radiated emissions," *IEEE Trans. Electromagn. Compat.*, vol. 31, no. 2, pp. 189–193, May 1989.

[2] J. L. Drewniak, T. H. Hubing, and T. P. V. Doren, "Investigation of fundamental mechanisms of common-mode radiation from printed circuit boards with attached cables," in *Proc. 1994 IEEE Int. Symp. Electromagn. Compat.*, Chicago, IL, pp. 110–115.

[3] J. L. Drewniak, F. Sha, T. H. Hubing, T. P. V. Doren, and J. Shaw, "Diagnosing and modeling common-mode radiation from printed circuit boards with attached cables," in *Proc. IEEE Int. Symp. Electromagn. Compat.*, Atlanta, GA, Aug. 1995, pp. 465–470.

[4] D. M. Hockanson, J. L. Drewniak, T. H. Hubing, and T. P. V. Doren, "FDTD modeling of common-mode radiation from cables," *IEEE Trans. Electromagn. Compat.*, vol. 38, no. 3, pp. 376–387, Aug. 1996.

[5] K. Eroglu, "A practical comparison of cabling effects on radiated emissions," in *Proc. 1999 IEEE Int. Symp. Electromagn. Compat.*, Seattle, WA, pp. 734–738.

[6] D. M. Hockanson, J. L. Drewniak, T. H. Hubing, T. P. V. Doren, F. Sha, and M. Wilhelm, "Investigation of fundamental EMI source mechanisms driving common-mode radiation from printed circuit boards with attached cables," *IEEE Trans. Electromagn. Compat.*, vol. 38, no. 4, pp. 557–566, Nov. 1996.

[7] F. B. J. Leferink and M. J. C. M. van Doorn, "Inductance of printed circuit board ground planes," in *Proc. 1993 IEEE Int. Symp. Electromagn. Compat.*, Dallas, TX, pp. 327–329.
[8] D. M. Hockanson, J. L. Drewniak, T. H. Hubing, T. P. V. Doren, F. Sha, C. W. Lam, and L. Rubin, "Quantifying EMI resulting from finite-impedance reference planes," *IEEE Trans. Electromagn. Compat.*, vol. 39, no. 4, pp. 286–297, Nov. 1997.
[9] C. L. Holloway and E. F. Kuester, "Net and partial inductance of a microstrip ground plane," *IEEE Trans. Electromagn. Compat.*, vol. 40, no. 1, pp. 33–46, Feb. 1998.
[10] M. Leone, "Design expression for the trace-to-edge common-mode inductance of a printed circuit board," *IEEE Trans. Electromagn. Compat.*, vol. 43, no. 4, pp. 667–671, Nov. 2001.
[11] F. B. J. Leferink, "Reduction of printed circuit board radiated emission," in *Proc. IEEE Int. Symp. Electromagn. Compat.*, Austin, TX, Aug. 1997, pp. 431–438.
[12] G. Dash, J. Curtis, and I. Straus, "The current-driven model-experimental verification and the contribution of I_{dd} delta to digital device radiation," in *Proc. IEEE Int. Symp. Electromagn. Compat.*, Seattle, WA, Aug. 1999, pp. 317–322.
[13] H. A. Wheeler, "Transmission-line properties of a strip on a dielectric sheet on a plane," *IEEE Trans. Microw. Theory Tech.*, vol. MTT-25, no. 8, pp. 631–647, Aug. 1977.
[14] S. A. Roy, "Simulation tools for the analysis of single electronic systems," Ph.D. dissertation, Dept., Electron. Elect. Eng., Univ., Glasgow, U.K., 1994.
[15] *COMORAN 2.5.0 User Guide*, Yokohama, Japan: Zuken, 2002.
[16] K. Nabors, S. Kim, J. White, and S. Senturia, *Fast Cap User's Guide.* Research Laboratory of Electronics, Department of Electrical Engineering and Computer Science. Cambridge, MA: Massachusetts Institute of Technology.
[17] K. Li, C. F. Lee, S. Y. Poh, R. T. Shin, and J. A. Kong, "Application of FDTD method to analysis of electromagnetic radiation from VLSI heatsink configurations," *IEEE Trans. Electromagn. Compat.*, vol. 35, no. 2, pp. 204–214, May 1993.
[18] C. E. Brench, "Heatsink radiation as a function of geometry," in *Proc. IEEE Int. Symp. Electromagn. Compat.*, Chicago, IL, Aug. 1994, pp. 105–109.
[19] J. F. Dawson, A. C. Marvin, A. Nothofer, J. E. Will, and S. Hopkins, "The effects of grounding on radiated emissions from heatsinks," in *Proc. IEEE Int. Symp. Electromagn. Compat.*, Montreal, QC, Canada, Aug. 2001, pp. 1248–1252.
[20] N. J. Ryan, D. A. Stone, and B. Chambers, "Application of FD-TD to the prediction of RF radiation from heatsinks," *Electron. Lett.*, vol. 33, no. 17, pp. 1443–1444, Aug. 14, 1997.
[21] T. Watanabe, S. Matsunaga, O. Wada, M. Kishimoto, T. Tanimoto, A. Namba, and R. Koga, "Equivalence of two calculation methods for common-mode excitation on a printed circuit board with narrow ground plane," in *Proc. IEEE Symp. Electromagn. Compat.*, Boston, MA, Aug. 2003, pp. 22–27.
[22] T. Watanabe, O. Wada, A. Namba, K. Fujimori, S. Matsunaga, and R. Koga, "Quantitative evaluation of common-mode radiation from a PCB based on imbalance difference model," in *Proc. IEEE Symp. Electromagn. Compat.*, Boston, MA, Aug. 2003, pp. 28–33.
[23] T. Hubing, N. Kashyap, J. Drewniak, T. V. Doren, and R. DuBroff, "Expert system algorithms for EMC analysis," in *Proc. 14th Annu. Rev. Progress in Applied Computational Electromagn.*, Monterey, CA, Mar. 1998, pp. 905–910.
[24] H. Shim, T. Hubing, T. V. Doren, R. DuBroff, J. Drewniak, D. Pommerenke, and R. Kaires, "Expert system algorithms for identifying radiated emission problems in printed circuit boards," in *Proc. 2004 IEEE Int. Symp. Electromagn. Compat.*, Santa Clara, CA, pp. 57–62.
[25] C. S. Walker, *Capacitance, Inductance and Crosstalk Analysis*. Boston, MA: Artech House, 1990.
[26] H. W. Shim, "Development of radiated EMI estimation algorithms for PCB EMI expert systems," Ph.D. dissertation, Univ. Missouri-Rolla, May 2004.

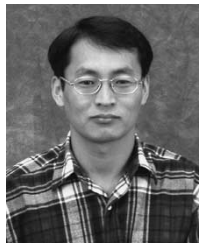

Hwan-Woo Shim was born in Kyungpook Province, Korea, in 1968. He received the B.E. degree from Kyungpook National University, Daegu, Korea, in 1991, the M.S. degree from Korea Advanced Institute of Science and Technology, Daejeon, Korea, in 1994, and the Ph.D. degree in electrical engineering from the University of Missouri–Rolla, in 2004.

In 1999, he joined the EMC Laboratory, University of Missouri–Rolla. From 1994 to 1999, he was with the Electronics and Telecommunication Research Institute, Daejeon, Korea. Since 2004, he has been with the Mobile Communication Division, Samsung Electronics Company, where he develops GSM mobile phones. His research interests include electromagnetic compatibility problems, advanced radio frequency measurements, and computational electromagnetics.

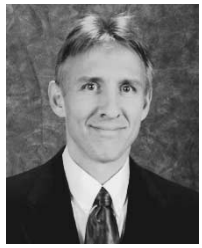

Todd H. Hubing (S'82–M'82–SM'93) received the B.S.E.E. degree from the Massachusetts Institute of Technology, Cambridge, in 1980, the M.S.E.E. degree from Purdue University, West Lafayette, IN, in 1982, and the Ph.D. degree in electrical engineering from North Carolina State University, Raleigh, in 1988.

He is currently a Professor of electrical engineering with the University of Missouri–Rolla (UMR), where he is also a member of the principal faculty in the Electromagnetic Compatibility Laboratory. Prior to joining UMR in 1989, he was an Electromagnetic Compatibility Engineer with IBM, Research Triangle Park, NC. Since joining UMR, the focus of his research has been on measuring and modeling sources of electromagnetic interference. He has authored or presented more than 100 technical papers, presentations, and reports on electromagnetic modeling and electromagnetic compatibility-related subjects. He is an Associate Editor of the *Journal of the Applied Computational Electromagnetics Society.*

Dr. Hubing was a member of the Board of Directors of the IEEE EMC Society from 1995 to 2005 and is a Past President of the society. He has also served as an Associate Editor of the IEEE TRANSACTIONS ON ELECTROMAGNETIC COMPATIBILITY.